

Atomic and electronic structure of ideal and reconstructed α -Sn (100) surfaces

Zhong-Yi Lu* and Guido L. Chiarotti

*International School for Advanced Studies (SISSA), Via Beirut 2, I-34014 Trieste, Italy
and Istituto Nazionale di Fisica della Materia (INFN), Trieste, Italy*

S. Scandolo and E. Tosatti

*International School for Advanced Studies (SISSA), Via Beirut 2, I-34014 Trieste, Italy;
Istituto Nazionale di Fisica della Materia (INFN), Trieste, Italy;
and The Abdus Salam International Centre for Theoretical Physics, P.O. Box 586, I-34014 Trieste, Italy*

(Received 29 January 1998)

α -Sn(100) surfaces have been recently produced through epitaxial growth of Sn on InSb (100). Reflection high-energy electron-diffraction data on these surfaces exhibit a variety of reconstructions with periodicities 2×1 , $p(2 \times 2)$, and $c(4 \times 4)$, attributed to possible ordering of dimers, in analogy to Si(100) and Ge(100) surfaces. Here we present a theoretical study of α -Sn(100) using the *ab initio* pseudopotential local-density approximation to search for the stable atomic and electronic structure. We find that surface dimers indeed form, accompanied by a large energy gain of 0.618 eV/(surface atom) with respect to the ideal surface. As in Si and Ge, the dimer is buckled, but in α -Sn the amount of buckling is surprisingly large, 1.0 Å, to be compared with 0.4 Å (Si) and 0.74 Å (Ge). A frozen phonon calculation predicts a corresponding surface dimer rocking mode at 4.8 THz. The surface core-level shift was found to be 0.6 eV for the up-dimer atom. In the ground state of α -Sn(100) we find that dimers tend to order “antiferromagnetically.” Calculations show that the most favored states with asymmetric buckled dimers are the $c(4 \times 2)$ and $p(2 \times 2)$ antiferro reconstructions, found to be nearly degenerate. Results are discussed in connection with existing and future experiments.

[S0163-1829(98)06143-8]

I. INTRODUCTION

The surface physics of α -Sn, a zero-gap semiconductor isostructural and isoelectronic to diamond, Si, and Ge, has long been uninvestigated, probably due to the unavailability of good crystals. Epitaxial growth of α -Sn on InSb has been reported by several experimental groups,^{1,2} with α -Sn film thicknesses as high as 2500 Å for α -Sn/InSb(100). Low-energy electron-diffraction (LEED) and reflection high-energy electron-diffraction (RHEED) data show that α -Sn(100) displays a variety of reconstructions, in particular a two-domain 2×1 , a $p(2 \times 2)$, and a $c(4 \times 4)$, which prevail successively for increasing film thicknesses on the InSb(100) substrate.² The same, or very similar, reconstructions are also present in Si(100) and Ge(100). It is now universally accepted that the reconstructions of these two surfaces fundamentally arise from the formation of surface dimers.³ In particular, asymmetric dimers are considered as building blocks for observed reconstructions such as 2×1 , $c(4 \times 2)$, $p(2 \times 2)$, and so on. The similarity in the reconstruction periodicities observed on α -Sn(100) to those of Si(100) and Ge(100) suggests that dimer-based reconstructions should also play a fundamental role on α -Sn(100). However, no direct evidence for the existence of dimers has been produced so far for α -Sn(100), nor has any quantitative hint been provided of their geometry, of the magnitude of the buckling (if any), and of the electronic and vibrational properties which would substantiate the dimer hypothesis.

We have therefore carried out a study of the atomic and electronic structure of α -Sn(100), in order to provide a sounder basis for further experimental investigations. Our

conclusion is that dimers are indeed formed and are stable on this surface. The main unexpected feature which we find is a giant magnitude of the asymmetric buckling, predicted to be as large as 1 Å, a factor of about 2.5 larger than that measured in Si(100).⁴ Related properties which we predict are a 1.2-eV surface gap, and a well-defined dimer surface resonance at relatively high frequency (4.8 THz) in the surface vibrational spectrum of α -Sn(100). As for the ground-state surface periodicity, among the possible high-order reconstructions $p(4 \times 1)$, $p(2 \times 2)$, $c(2 \times 2)$, $c(4 \times 2)$, and $c(4 \times 4)$ we find that the lowest energies are $c(4 \times 2)$ and $p(2 \times 2)$, found to be nearly degenerate. The energy spread among these possibilities is of the order of 0.1 eV per dimer, and can be modeled by an effective Ising Hamiltonian.

II. CALCULATIONAL TECHNIQUES

The calculations have been performed using the *ab initio* pseudopotential plane-wave self-consistent method, based on the density-functional theory within the local-density approximation (LDA).⁵ We adopted the Ceperley-Alder exchange and correlation functional with the parametrization of Perdew and Zunger,⁶ and modeled the electron-ion interaction using a norm-conserving pseudopotential⁷ in Kleinman-Bylander form,⁸ with *s* and *p* nonlocalities. The Kohn-Sham orbitals were expanded in plane waves with an energy cutoff of 12 Ry. As shown in Ref. 9, this approach yields, among other properties, the correct relative energy ordering of bulk α -Sn and β -Sn, the transition pressure between these two phases, and their electronic band structures.

We modeled the surface (unless otherwise specified) us-

ing a periodically repeated slab of 12 Sn monolayers with inversion symmetry through the center of the slab, and a vacuum layer of 11 Å. The initial atomic positions are chosen according to the calculated⁹ equilibrium bulk lattice spacing [$a_o = 6.446$ Å, quite close to the experimental value 6.483 Å (Ref. 10)]. We froze the two innermost middle layers, but allowed all other atoms to relax according to the calculated Hellmann-Feynman forces. The relaxation was terminated when the forces were less than 5 meV/Å.

A set of four special k points was chosen to sample the 2×1 rectangular irreducible surface Brillouin zone (ISBZ).¹¹ For calculations involving different surface unit cells, we chose a set of k points equivalent to the four special points of the 2×1 ISBZ: specifically, eight k points for the 1×1 ISBZ, four k points for the 2×1 symmetric-dimer ISBZ, eight k points for the 2×1 asymmetric-dimer ISBZ due to the dimer's breaking mirror symmetry, two k points for $p(4 \times 1)$, four k points for $p(2 \times 2)$, eight k points for $c(2 \times 2)$, and four k points for $c(4 \times 4)$. An equivalent k -point sampling cannot be found for the $c(4 \times 2)$ oblique ISBZ, and we therefore sampled the $c(4 \times 2)$ oblique ISBZ with four special k points. In order to check the convergence properties of our k -point sampling, we repeated the calculation of the Hellmann-Feynman forces at the end of the relaxation, for all considered reconstructions, doubling the number of k points. No meaningful changes took place on any of the structures. In the case of metallic surfaces, we used a Gaussian broadening of 0.001 Ry, according to Ref. 12.

From the construction of our slab, the surface energies E_{surf} are defined as

$$E_{surf} = (E_{slab} - NE_{bulk})/2, \quad (1)$$

where E_{slab} is the total energy of the slab, E_{bulk} is the energy per atom of bulk α -Sn, N is the total number of atoms in the slab, and the factor $\frac{1}{2}$ accounts for the two identical surfaces, as required by inversion symmetry. In order to minimize the errors introduced by the finite k -point sampling in Eq. (1), the value of E_{bulk} was recalculated for each surface reconstruction, using the same supercell and k -point sampling adopted for the surface calculations.¹³ In practice, this amounted to perform two independent supercell calculations for the bulk α -Sn energy E_{bulk} using the 2×1 slab cell and the $c(4 \times 2)$ slab cell, respectively. The calculated energies per atom of bulk α -Sn E_{bulk} are -96.773 eV/atom in the 2×1 slab case, and -96.757 eV/atom in the $c(4 \times 2)$ slab case.

Vibrational contributions, both in the form of zero-point motion and in the form of finite-temperature entropic contributions, are not included in the evaluation of surface energies. Although a full phonon spectrum calculation would in principle be necessary for a quantitative determination of both contributions, differences in the vibrational spectra of various reconstructions have been found to be minimal in Si(100),^{14,15} and we do not expect qualitative differences for Sn(100). For most of these surfaces we computed, among other quantities, the surface work function, the layer-projected density of states, and the core-level shifts in the outermost atoms.

Surface work function: The surface work function ϕ , although rarely calculated, represents an important electronic

property of a surface, and one that can be directly measured in experiments. It is defined as $\phi = \bar{V}_H(\text{vacuum}) - E_F$, where E_F is the Fermi energy and $\bar{V}_H(\vec{r})$ is the macroscopic average of the Hartree potential $V_H(\vec{r})$. The Hartree potential $V_H(\vec{r})$ satisfies Poisson's equation

$$\nabla^2 V_H(\vec{r}) = 4\pi\rho(\vec{r}), \quad (2)$$

and can be easily obtained from the self-consistent electronic charge density. Following the approach proposed by Baldereschi, Baroni, and Resta,¹⁶ we compute the average \bar{V}_H in the form

$$\bar{V}_H(z) = \frac{1}{aS_0} \int_{z-a/2}^{z+a/2} ds \int_{S_0} dx dy V_H(x, y, s), \quad (3)$$

where S_0 is the surface unit area, a is the α -Sn bulk lattice parameter, and z is the coordinate normal to the surface. Physically, of course, we expect $\bar{V}_H(z)$ to be constant in the vacuum and also in the central, bulklike, region of the slab.

Layer-projected density of states (LDOS): In real space, at position \vec{r} , the local density of states $\rho(\vec{r}, E)$ of the slab is defined as

$$\rho(\vec{r}, E) = \sum_n \int_{SBZ} d\vec{k} |\Psi_k^{(n)}(\vec{r})|^2 \delta[E - E_n(\vec{k})], \quad (4)$$

where n is the band index, SBZ denotes the surface Brillouin zone, $\Psi^{(n)}$ and E_n are the eigenstate and eigenvalue of the n th band, respectively. The LDOS can be projected onto the different layers in the slab as follows:

$$\begin{aligned} \rho(m, E) = & \sum_n \int_{SBZ} d\vec{k} \int_{S_0} dx dy \\ & \times \int_{z_m - \Delta/2}^{z_m + \Delta/2} dz |\Psi_k^{(n)}(x, y, z)|^2 \delta[E - E_n(\vec{k})], \end{aligned} \quad (5)$$

where z_m denotes the m th layer position, and Δ is the distance between the two nearest neighbor layers. This LDOS will resemble the bulk density of states $\rho(E)$ in the slab center, but it will display surface-state effects in the outer layers. The LDOS is a useful quantity and can be used to interpret several experiments, including photoemission and scanning tunneling microscopy. In our calculation, due to the finite resolution of our k -point sampling, we replaced the δ function in formula (5) by a Gaussian function with a broadening of 25 meV.

Surface core-level shift (SCLS): The surface core-level shift relative to the bulk is easily measured in photoemission experiments, and is a relevant quantity to understand the local environments of atoms. It is defined as the difference between the kinetic energies of an electron emitted from a given core shell of a surface atom and from the same shell of a bulk atom, when they are excited with the same photon energy. Two different theoretical frameworks are typically followed to evaluate the SCLS: the initial-state picture and the final-state picture.¹⁷ The initial-state picture assumes that the SCLS is equal to the difference between the single-particle energy eigenvalues of a core state in a surface atom

TABLE I. Parameters for the Sn pseudopotential with a screened $4d$ hole. Energies in Ry.

| Sn ⁺ | $l=0$ | $l=1$ | $l=2$ |
|-----------------|-----------|-----------|-----------|
| α_c | 0.654040 | | |
| α_l | 0.976805 | 0.646154 | 0.741125 |
| a_l | 11.861162 | 4.295659 | -0.211686 |
| b_l | -5.005743 | -1.085313 | 1.358163 |

and a bulk atom prior to removal. By definition, the initial-state picture does not consider the core-relaxation (screening) effect of the core level, which is instead included in the final-state picture. In this paper we evaluated SCLS's in both pictures, following the approach of Refs. 17 and 18. For the initial-state picture, we first averaged the obtained self-consistent potential (Hartree potential plus exchange-correlation potential) in a sphere centered on each considered surface and bulk atom (in our calculations the center-layer atoms are considered as the bulk atoms). The radius of the sphere was chosen to be slightly larger than half the bulk bond length.¹⁹ Then the SCLS was evaluated as the difference between the averaged potentials in the surface atom and the bulk atom. For the final-state picture, we first must generate a pseudopotential with a $4d$ hole (for α -Sn, $4d$ electrons are usually detected in photoelectron spectroscopy experiments).²⁰ This was done following the method of von Barth and Car,²¹ where the ‘‘core-hole’’ pseudopotential is given in a norm-conserving semilocal form by

$$V_l(r) = -\frac{Z_v}{r} \text{erf}(\sqrt{\alpha_c} r) + (a_l + b_l r^2) e^{-\alpha_l r^2}, \quad (6)$$

where l denotes the angular momentum, Z_v is the core valence charge ($Z_v=5$ in this case). The parameters α_c , a_l , and b_l , obtained by a fitting procedure,²² are reported in Table I. Transferability for this pseudopotential has been tested for several excited configurations of the Sn atom, such as s^3p^1 , s^1p^3 , $s^2p^1d^1$, $s^1p^2d^1$, s^2p^1 , and s^1p^2 . We then performed two self-consistent calculations by substituting the original pseudopotential with the ‘‘core-hole’’ one in the

considered surface and bulk atoms, respectively. Accordingly, the SCLS is the difference in the total energies between these two calculations with the core hole.

III. UNRECONSTRUCTED α -SN(100) SURFACE

We started by considering the ideal α -Sn(100) surface, where all atoms are in a truncated bulk position. This calculation serves to identify the basic driving forces toward more stable reconstructions, and also as a reference state. The calculated α -Sn ideal (100) surface energy turns out to be 1.530 eV/(1×1 cell) (Table II). The corresponding ideal surface electronic band structure is reported in Fig. 1. It is seen that half-filled surface bands cross the gap regions of the projected bulk energy bands. In particular, since, on the ideal α -Sn(100) surface, each surface atom has two dangling bonds, the latter gives rise to two surface-state bands in the fundamental gap region. The splitting between these two surface-state bands indicates a non-negligible interaction between the two dangling bonds, lifting their original degeneracy. This is also reflected by electron charge density maps in two upper panels of Fig. 1, which correspond to the square amplitude of surface states S_1 and S_2 at point \bar{K} , namely, so-called dangling-bond state and bridge-bond state, respectively. An inspection of the total electron charge-density distribution²³ shows that in the ideal surface there is no bond formation among neighboring surface atoms so long as they are kept frozen, and the electrons are highly localized around them. The protrusive character of these electronic states suggests that the work function of the ideal α -Sn(100) surface should be rather high. We computed the planar and macroscopic averages of the Hartree potential, and obtained a value for the work function of 4.68 eV (the values of all calculated work functions are reported in Table III). We also calculated the surface LDOS (the right panel of Fig. 1), which shows that the main weights of S_1 and S_2 are clearly located at the two sides of the Fermi level. Therefore, even though the Fermi level crosses the surface bands in the fundamental gap (see Fig. 1), the ideal α -Sn(100) surface displays a nearly negligible density of states at the Fermi level, much like the ideal Si(100) (Ref. 24) surface, owing to a large dispersion of

TABLE II. Calculated surface energies, absolute E_{surf} and relative ΔE , dimer buckling b , dimer buckling angle ω , and dimer bond length d of different optimized reconstructions for the α -Sn(100) surface. In the table SMD indicates single missing dimer.

| Structure | E_{surf} [eV/(1×1 cell)] | [mJ/m ²] | ΔE [eV/(1×1 cell)] | b (Å) | ω | d (Å) |
|---------------------------|---|----------------------|---|------------|----------|------------|
| ideal | 1.530 | 1180 | 0.000 | | | |
| fully relaxed | 1.507 | 1162 | -0.023 | | | |
| 2×1 symmetric | 1.031 | 795 | -0.499 | 0 | 0° | 2.90 |
| SMD- p (2×2) | 0.995 | 767 | -0.535 | 1.05 | 21.15° | 2.91 |
| SMD- c (4×4) | 0.970 | 748 | -0.560 | 1.09 | 22.29° | 2.87 |
| 2×1 asymmetric | 0.912 | 703 | -0.618 | 1.01 | 20.99° | 2.82 |
| p (4×1) | 0.909 | 701 | -0.621 | 0.964 | 20.06° | 2.81 |
| c (2×2) | 0.907 | 699 | -0.623 | 1.03 | 20.88° | 2.89 |
| c (4×4) | 0.903 | 696 | -0.627 | 1.02 | 20.80° | 2.87 |
| c (4×2) | 0.873 | 673 | -0.657 | 1.06 | 21.67° | 2.87 |
| p (2×2) | 0.872 | 672 | -0.658 | 1.06 | 21.60° | 2.88 |

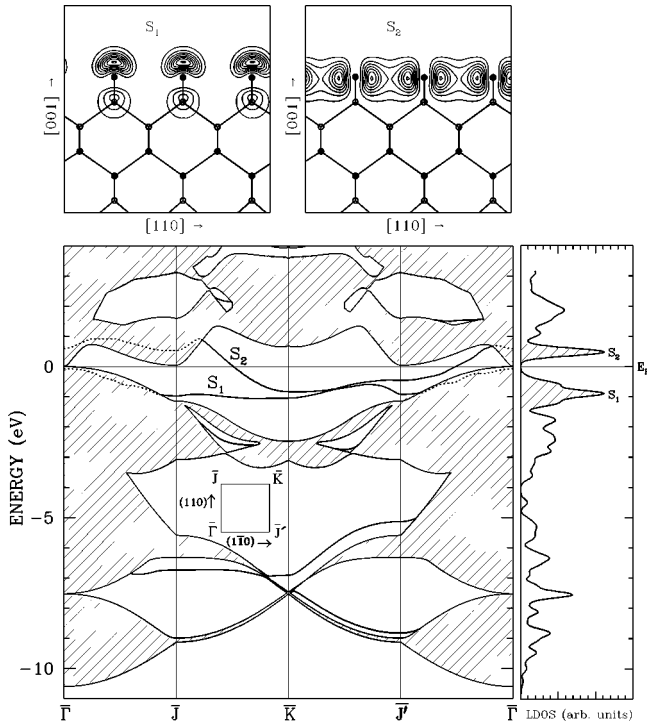


FIG. 1. Surface electronic band structure of the ideal α -Sn(100) surface reported along high-symmetry lines of the 1×1 square irreducible Brillouin zone. The broken bonds lie in the (110) plane. Shaded areas correspond to surface-projected bulk states. Thicker lines correspond to surface states, and dotted lines to surface resonances. The irreducible surface Brillouin zone is given in the inset. Note the large dispersion of the partly filled surface state bands S_1 and S_2 associated with the broken bonds. The two upper panels display the electron-density contours of the surface S_1 (upper left panel) and S_2 (upper right panel) eigenstates at \bar{K} on the (110) plane passing through the Sn atoms represented by full circles. Empty circles indicate the out-of-plane Sn atoms, and thicker straight lines to bonds among Sn atoms. Contour lines are separated by 0.002 a.u. Note the much higher degree of electron charge localization on top atoms for state S_1 , compared to S_2 . The right panel displays the layer-projected density of states (LDOS) projected on the surface layer with the same energy scale as that of the left electronic band structure on the vertical axis. Shaded areas indicate the surface states. Note the nearly zero density of states at the Fermi level.

the surface bands in the fundamental gap. Nevertheless, the very high value of the surface energy, as well as the presence of surface states with a high degree of electron charge localization, suggest that this ideal surface should be unstable toward relaxation and/or reconstruction, as on Si(100) and Ge(100).

The atomic positions in the slab were at first allowed to

TABLE III. Calculated work functions Φ , respectively, for the 2×1 asymmetric dimer reconstructed surface, the 2×1 symmetric dimer reconstructed surface, and the ideal unreconstructed α -Sn(100) surface.

| Structure | Asymmetric dimer | Symmetric dimer | Ideal |
|-------------|------------------|-----------------|-------|
| Φ (eV) | 4.43 | 4.42 | 4.68 |

relax still preserving the 1×1 surface periodicity. This led to a gain in surface energy of only 23 meV/(1×1 cell) and a small vertical inward relaxation of only 0.071 Å in the surface atoms, indicating that only proper reconstructions with higher periodicity are likely to lower the energy. In the following sections we consider the possible reconstructions of α -Sn(100) with larger surface unit cells.

IV. 2×1 DIMER RECONSTRUCTIONS

A. 2×1 symmetric dimer

Our approach is to ignore at first the subtleties related to higher periodicities, and focus on the understanding of the basic building block of all (100) reconstructions, particularly the possible formation of surface dimers. Accordingly we first restricted our analysis to a 2×1 surface unit cell. We constructed a trial symmetric dimer structure in which the two surface atoms are dimerized, and all bond lengths, including the dimerized bond, are initially set equal to the bulk bond length. We also require a mirror symmetry along $[1\bar{1}0]$ to be preserved in our slab so as to preserve the initial symmetry between neighboring surface atoms. As it turns out, it is impossible to have a mirror symmetry in a slab of 12 layers with inversion symmetry, while this can be done with 10 or 14 layers. In the present calculation, we chose a slab of 14 layers with inversion symmetry across its middle bilayer, plus the required mirror symmetry along $[1\bar{1}0]$. In this case we froze the atoms in the four innermost layers, and relaxed all the others.

Full relaxation of the atomic positions in the 2×1 symmetric dimer reconstruction so obtained leads, as expected, to a dramatic lowering of surface energy to 1.031 eV/(1×1 cell), which is 0.499 eV/(1×1 cell) lower than the ideal surface (see Table II). This lowering is related to the formation of the Sn-Sn surface dimer bond, which reduces the number of the dangling bonds from two to one per surface atom. An inspection of the total electron charge density²³ confirms that a strong bond forms in the surface dimer. The band structure and surface LDOS (Fig. 2), however, show that the surface is still metallic, similar to the symmetric dimer Si(100) and Ge(100) surfaces,^{25–28} due to the remaining dangling bonds. This is made clear by the squared wave functions of the metallic surface states S_1 and S_2 at \bar{K} , reported in Fig. 3. The mirror symmetry between the two residual dangling bonds is clearly seen. Besides the surface bands S_1 and S_2 , there are other surface bands S_3 , S_4 , and S_5 in the fundamental gap region, which will similarly appear in the following asymmetric dimer case and will be discussed there. The final relaxed atomic coordinates for the symmetric dimer calculation are given in Ref.23. The dimer bond length is 2.90 Å (the bulk bond length is 2.79 Å). Charge-density maps²³ indicate that the electrons are more smoothly distributed around the top surface atoms than on the ideal α -Sn(100). The calculated surface work function turns out to be 4.42 eV, smaller than that of the ideal α -Sn(100), as expected from the increased smoothness of the electronic charge. The presence of half-filled dangling bonds and of metallic surface bands in the fundamental gap as usual suggests that the symmetric

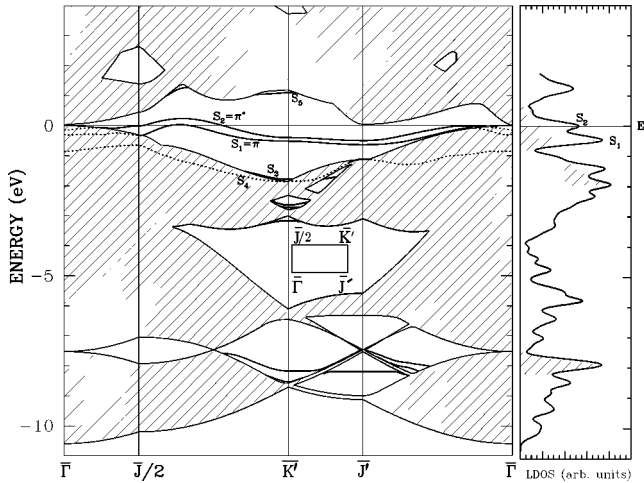


FIG. 2. Surface electronic band structure of the 2×1 symmetric dimer-reconstructed surface reported along high-symmetry lines of the 2×1 rectangular irreducible Brillouin zone. Shaded areas correspond to surface-projected bulk states, while thicker lines correspond to surface states. The irreducible surface Brillouin zone is given in the inset. Note the quasidegenerate surface bands S_1 and S_2 primarily distributed nearby the Fermi level, and its metallic feature. The right panel displays the layer-projected density of states (LDOS) projected on the surface layer with the same energy scale as that of the left electronic band structure on the vertical axis. Shaded areas indicate the surface states. Note the “good” metallic feature of the LDOS.

dimer reconstruction should still be unstable toward distortions, able to lift the residual near-degeneracy of the surface states S_1 and S_2 .

B. 2×1 asymmetric dimer

We next allowed the two surface atoms to become non-equivalent, thereby breaking the $[1\bar{1}0]$ mirror symmetry. We calculated the Hellmann-Feynman forces to guide the relaxation of the atomic structure. Even though the inequivalence of the surface atoms was initially minute, it grew to a considerable buckling immediately after relaxation.

The surface energy was very substantially lowered by asymmetrization of the dimer. Full relaxation of the atomic positions in the 2×1 *asymmetric* dimer reconstruction leads to a final surface energy of $0.912 \text{ eV}/(1 \times 1 \text{ cell})$, which is $0.119 \text{ eV}/(1 \times 1 \text{ cell})$ lower in energy than the symmetric case, and $0.618 \text{ eV}/(1 \times 1 \text{ cell})$ lower in energy than the ideal surface. The atomic coordinates of the fully relaxed asymmetric dimer reconstruction are reported in Table IV. This large energy gain is accompanied by a giant buckling of the dimer ($b = 1 \text{ \AA}$, $\omega = 21^\circ$).

The surface electronic band structure of the asymmetric dimer structure is reported in Fig. 4. As expected, the large buckling of the surface dimer leads to the opening of a large surface energy gap between surface bands S_1 and S_2 , compared with the symmetric dimer case (Fig. 2). The Fermi level lies in this gap, and the asymmetric dimer reconstruction is “insulating,” except for the zero-gap region near Γ . The buckling of the surface dimer causes the sp^3 covalent orbitals of the surface atoms to dehybridize partially. The

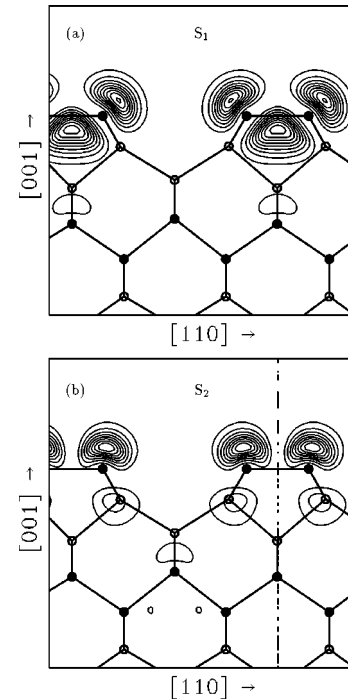


FIG. 3. Electron-density contours of the surface S_1 eigenstate (upper panel, π state) and of the surface S_2 eigenstate (lower panel, π^* state) in the 2×1 symmetric dimer reconstruction at \bar{K} , on the (110) plane passing through the Sn atoms represented by full circles. Empty circles indicate the out-plane Sn atoms, and thicker straight lines bonds among Sn atoms. Contour lines are separated by 0.0005 a.u. Note the mirror symmetry between the two dimer atoms.

TABLE IV. Optimized atomic positions of the α -Sn(100) asymmetric dimer (2×1)-reconstructed surface, and the corresponding bulklike (Ideal) positions. In the rectangular supercell, coordinates are given by $\mathbf{r} = c_1 \mathbf{a}_1 + c_2 \mathbf{a}_2 + c_3 \mathbf{a}_3$, where \mathbf{a}_i is defined in the conventional cubic coordinate system as $\mathbf{a}_1 = (a_0/2)(1, 1, 0)$, $\mathbf{a}_2 = (a_0/2)(1, -1, 0)$, and $\mathbf{a}_3 = a_0(0, 0, -1)$ with $a_0 = 12.181 \text{ a.u.} = 6.446 \text{ \AA}$ the α -Sn lattice parameter. The unit cell has one asymmetric dimer.

| | Atom no. | Ideal | | | Optimized | | |
|-------------|----------|-------|-------|-------|-----------|-------|-------|
| | | c_1 | c_2 | c_3 | c_1 | c_2 | c_3 |
| dimer-layer | | | | | | | |
| dimer-down | 1 | 0.500 | 0.250 | 1.375 | 0.500 | 0.550 | 1.266 |
| dimer-up | 2 | 0.500 | 1.250 | 1.375 | 0.500 | 1.128 | 1.423 |
| 2nd-layer | | | | | | | |
| | 3 | 0.000 | 0.250 | 1.125 | 0.000 | 0.247 | 1.133 |
| | 4 | 0.000 | 1.250 | 1.125 | 0.000 | 1.208 | 1.154 |
| 3rd-layer | | | | | | | |
| | 5 | 0.000 | 0.750 | 0.875 | 0.000 | 0.755 | 0.859 |
| | 6 | 0.000 | 1.750 | 0.875 | 0.000 | 1.717 | 0.899 |
| 4th-layer | | | | | | | |
| | 7 | 0.500 | 0.750 | 0.625 | 0.500 | 0.740 | 0.612 |
| | 8 | 0.500 | 1.750 | 0.625 | 0.500 | 1.744 | 0.642 |

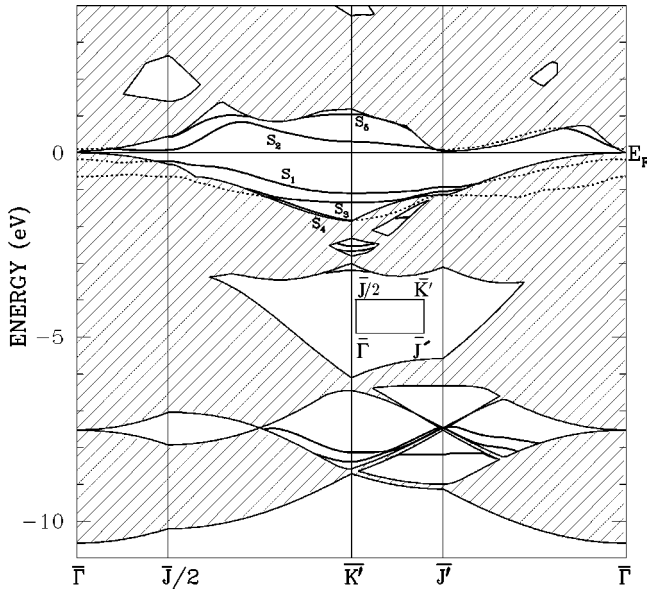


FIG. 4. Surface electronic band structure of the 2×1 asymmetric-dimer-reconstructed surface reported along high-symmetry lines of the 2×1 rectangular irreducible Brillouin zone. The Fermi level is set to zero. Shaded areas correspond to surface-projected bulk states, while thicker lines correspond to surface states. The irreducible surface Brillouin zone is given in the inset. Note the surface bands S_1 and S_2 , well separated in energy due to the large buckling between the dimer atoms, and the Fermi level in between them.

dangling bonds on the outward and inward surface atoms here become prevalently s and p like, respectively. According to the usual mechanism, some nominal electronic charge transfer from the p -like to the s -like dangling bond takes place. The completely filled surface states labeled with S_1 in the surface band structure of Fig. 4 are mainly localized on the outward surface atom with mostly s -like character (Fig. 5, upper panel), and the empty surface states labeled with S_2 are mainly localized on the inward surface atom with mostly p -like character (Fig. 5, lower panel). By analyzing the electron charge density distributions of the other surface bands S_3 , S_4 , and S_5 (Ref. 23) present in the fundamental gap region, we found that the filled surface states S_3 and the empty surface states S_5 are “back bond” surface states related to the second surface layer atoms. The surface band S_4 is instead closely related to the bond formed in the asymmetric buckled dimer.

The calculated LDOS for the asymmetric dimer surface is reported in Fig. 6. The surface states around the Fermi level in the right panel of Fig. 2 are split into two components, and are pushed at the two sides of the Fermi level. Both the LDOS and the surface band structure show that a gap of about 1.2 eV separates the two surface bands in the asymmetric dimer reconstruction of α -Sn(100). It is therefore predicted that a surface optical absorption peak should be observed at this frequency with surface-sensitive techniques such as infrared reflectivity, electron-energy loss spectroscopy (EELS), or photoemission, due to excitations across this gap.

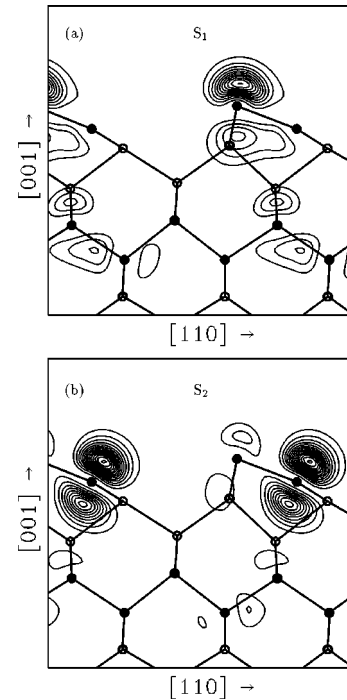


FIG. 5. Electron-density contours of the filled surface S_1 eigenstate (upper panel) and of the empty surface S_2 eigenstate (lower panel) in the 2×1 asymmetric dimer reconstruction at \bar{K} , on the (110) plane passing through the Sn atoms represented by full circles. Empty circles indicate the out-plane Sn atoms, and thicker straight lines bonds among Sn atoms. Contour lines are separated by 0.0005 a.u. Note the strong s -like state feature in the upper panel, and the strong p -like state feature in the lower panel.

V. PROPERTIES OF THE ASYMMETRIC-DIMER-RECONSTRUCTED α -Sn(100) 2×1

A. Surface rocking vibration

The effective dipole connected with the dimer buckling will be strongly modulated by a particular surface vibration, the “rocking mode,”¹⁴ which modulates the buckling. We have extracted an approximation to the eigenvector of this mode by examining the coordinate evolution in the last few steepest-descent iterations during relaxation, from zero buckling to the final large buckling geometry. Using this approximate eigenvector, we have calculated the frozen-phonon frequency (ν_r) of the rocking mode at $k=0$, and found $\nu_r = 4.8$ THz. The bulk zone-center Raman phonon frequency (ν_b) of α -Sn, calculated by constructing the eigenvector in the same way, is $\nu_b = 5.97$ THz, in excellent agreement with the experimental value $\nu_b = 6.0$ THz.²⁹ The dipole-active rocking mode is expected to resonate with bulk vibrations, falling, however, in a region of relatively low bulk density of phonon states²⁹ (see Fig. 7). We thus expect that it should be observable in high-resolution EELS. It is of interest to note that the same rocking mode is predicted to lie, in the asymmetric buckled structure of Si(100),¹⁴ at $\nu_r \sim 6$ THz, much below the bulk zone-center Raman phonon ($\nu_b \sim 16$ THz) making detection more difficult in that case. This predicted difference is attributable to the much stronger buckling of the α -Sn dimer.

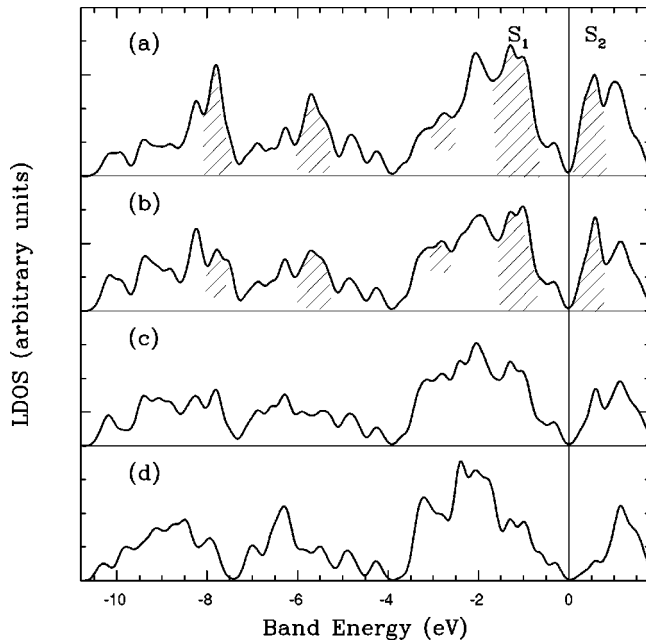


FIG. 6. Layer-projected density of states (LDOS) for the 2×1 asymmetric-dimer-reconstructed α -Sn (100) surface. The Fermi level is set to zero. In panels (a), (b), (c), and (d), the solid curves are, respectively, the density of states (DOS) projected on the surface layer, the second layer, the third layer and the center layer (sixth layer), whereas the DOS projected on the center layer produced a good bulk DOS. The LDOS of panel (c) very similar to that of panel (d), indicating surface states primarily related to surface-layer and second-layer reconstructions. Shaded areas indicate the surface states. Note the insulating feature of the LDOS in panel (a).

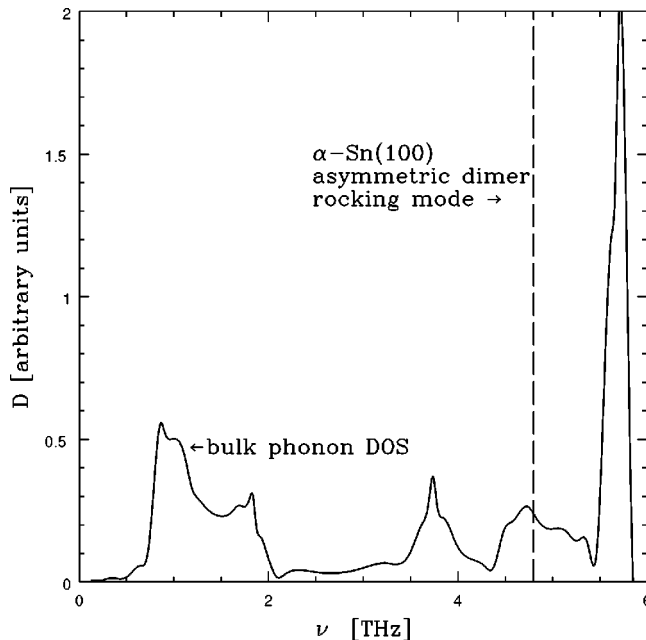


FIG. 7. The phonon spectrum for α -Sn, cited from Ref. 29. The added dashed line indicates the location of the α -Sn(100) asymmetric dimer rocking mode. Note that the predicted rocking mode lies in the low bulk phonon density of states (DOS) region.

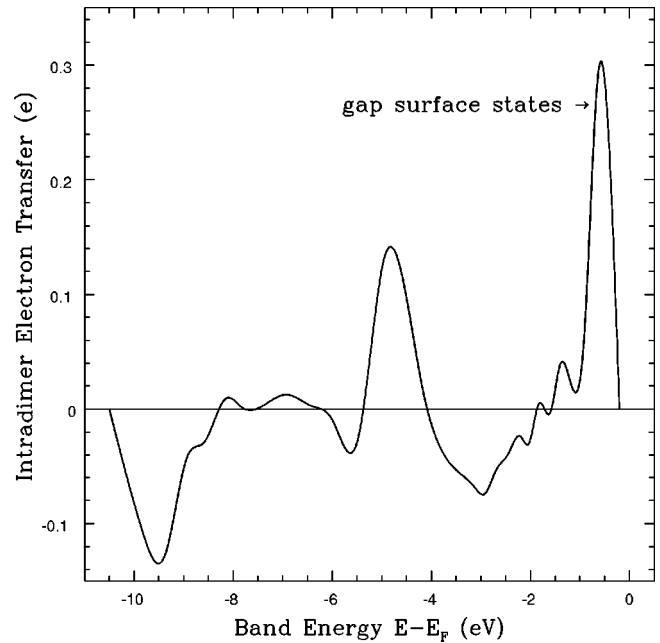


FIG. 8. The calculated charge transfers from the down-dimer atom to the up-dimer atom, corresponding to the different energy bands for the α -Sn(100) 2×1 asymmetric dimer reconstruction. Here the vertical axis indicates the charge transfer (units in e), while the other axis indicates the band energies (units in eV). The Fermi level is set to zero.

B. Net static charge transfer

The computed work function for this asymmetric dimer surface is 4.43 eV, very much the same as that of the symmetric dimer surface. This fact seems to indicate that the asymmetrization, although giant, does not induce any true, net charge transfer (which would increase the surface work function in the absence of screening effects), and correspondingly screening effects are indeed strong and a naive picture of pure charge transfer does not apply.

In order to clarify this situation, we carefully computed the charge transfers from the down-dimer atom to the up-dimer atom corresponding to the different energy bands. We respectively integrated the self-consistent electronic charge densities of the different energy bands in the spheres centered on the down-dimer and up-dimer atoms with a radius slightly larger than the half of the bulk bond length.³⁰ The charge transfer is, therefore, the difference between the above two integrations around the up and down atoms. The energy-resolved charge transfer is reported in Fig. 8. We see that a considerable amount of charge transfer indeed takes place in the surface states. However, this is almost completely compensated for by a charge backflow, clearly associated with a rehybridization of back bonds which restores the net average value close to zero.

C. Surface core-level shifts

The inequivalence of the two dimer atoms connected with the formation of such a large buckling should give rise to an observable shift in the core-level position of the dimer atoms. We therefore computed the core level shifts on the 2×1 asymmetric dimer reconstruction, which are reported in Table V.

TABLE V. Calculated surface core-level shifts on the considered atoms for the 2×1 asymmetric buckled dimer reconstruction in the initial- and final-state pictures. The shift is relative to a bulk atom. Units are in eV. Here 2nd layer atom indicates one of the second-layer atoms, which goes up slightly.

| | Initial state | Final state |
|-----------------|---------------|-------------|
| up-dimer atom | 0.77 | 0.61 |
| down-dimer atom | -0.01 | -0.10 |
| 2nd-layer atom | 0.38 | 0.44 |

We note that surface core-level shifts are nearly identical in both initial- and final-state approximations. The core-level shift is close to zero for the down atoms, and 0.6–0.8 eV lower binding energies for the up atoms. This predicted value is close to that of rest atoms on Si(111) and Ge(111), and, in analogy with those, can be associated with the presence of an extra polarizable charge on the atom. It should be noted that the shift would be much larger if the overall buckling-induced charge transfer driven by surface states were not compensated for by the backflow described in Sec. V B.

VI. HIGHER RECONSTRUCTIONS BASED ON THE ASYMMETRIC DIMERS

In Si(100) and Ge(100) a variety of higher reconstructions are observed,^{31–35} such as 2×1 , $c(4 \times 2)$, $p(2 \times 2)$, $c(2 \times 2)$, $c(4 \times 4)$, and $2 \times n$, where $6 < n < 10$. Several of them sometimes coexist. The 2×1 reconstruction is the room-temperature phase. The $2 \times n$ reconstructions ($6 < n < 10$) are obtained by rapid quenching from high temperatures, are metastable, and decay with a first-order kinetics.³² Exposing 2×1 surfaces to hydrogen, and annealing at 570–690 °C, induces the formation of a $c(4 \times 4)$ reconstruction on Si(100).^{36,37} Finally, the $c(4 \times 2)$, $p(2 \times 2)$, and $c(2 \times 2)$ reconstructions predominate at low temperatures. As for the ground state, theoretical calculations^{38,27,28} and experiments^{33,35} agree in that the $c(4 \times 2)$ or $p(2 \times 2)$ are nearly degenerate.

Pandey³⁹ proposed a “missing dimer defect” model to account for the observed complicated reconstructions on (100) surfaces. However, *ab initio* calculation by Roberts and Needs²⁸ showed the missing dimer defect model to be energetically higher than the 2×1 asymmetric dimer model. Currently, only the metastable reconstructions $2 \times n$ ($6 < n < 10$) and $c(4 \times 4)$ are tentatively explained in terms of the missing dimer defect model: the former as the ordering of excess missing dimer defects,³² the latter as an ordered structure with missing dimer defects formed on the basic 2×1 structure.³⁷ The stable reconstructions 2×1 , $c(4 \times 2)$, $p(2 \times 2)$, and $c(2 \times 2)$ are instead believed to be formed by different arrangements of two nonequivalent “antiferro” asymmetric dimers (see Fig. 9).

Generally speaking, reconstructions based on asymmetric dimers as building blocks can be classified, according to the group theoretical argument,^{40,41} into three families, namely, a “ 2×1 ” family with a 2×1 backbone, a “ 2×2 ” family with a 2×2 backbone, and a “ $c(2 \times 2)$ ” family with a $c(2 \times 2)$ backbone. Among these, the reconstructions be-

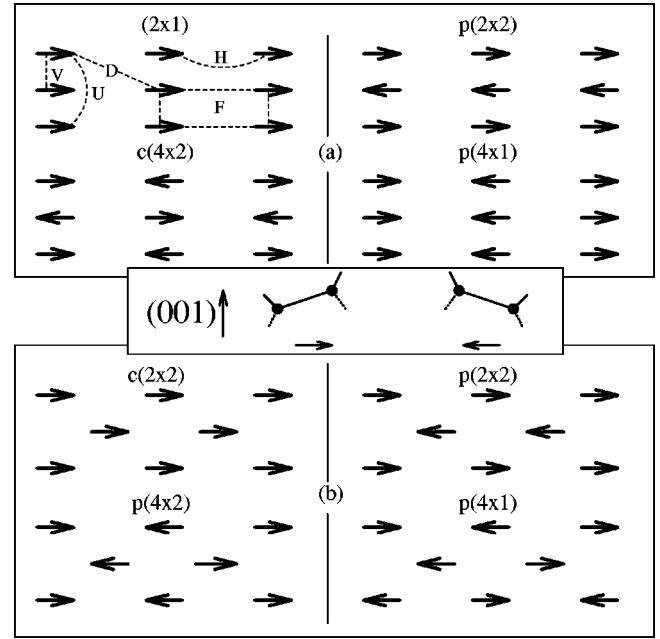


FIG. 9. Arrangements of asymmetric buckled dimers on α -Sn(100) for the 2×1 family (a), and $c(2 \times 2)$ family (b), cited from Ref. 38. Side views of the oppositely oriented asymmetric dimers are shown in the inset. Coupling constants corresponding to the mapped Ising Hamiltonian (7) are indicated for the 2×1 family (a).

longing to the 2×2 family have only one-half of the surface atoms dimerized in their unit cells, and they are never observed in experiments. The typical reconstruction geometries of the 2×1 and $c(2 \times 2)$ families are instead schematically shown in Fig. 9.

The surface energies of reconstructions belonging to the same family are very similar, and their structures are connected by transformation paths that do not involve breaking of bonds among the surface and bulk. Thus structural transitions within each family can readily take place. For Si(100) and Ge(100) surfaces, the surface energies of the $c(2 \times 2)$ family are higher than those of 2×1 family.³⁸ Moreover, structural transitions from the $c(2 \times 2)$ family to the 2×1 family are hindered, since a large amount of energy is needed to break and displace the strong dimer bonds and the bonds related to the domain walls when these two families of reconstructions coexist on the surfaces. In practice, the realization of a given reconstruction strongly depends upon the surface-preparation conditions. In some special conditions, both 2×1 and $c(2 \times 2)$ families can be created on the same surface with stable domain walls among them.^{42,33}

The recent RHEED experiment by Yuen *et al.*² also discovered reconstructions such as two-domain 2×1 , $p(2 \times 2)$, and $c(4 \times 4)$ on α -Sn(100) surfaces. These reconstructions were observed to occur in this sequence during growth on InSb(100), and no attempt to understand their origin or relative stability was made. It is tempting to assign these reconstructions on Sn(100) to the same mechanisms proposed for Si(100) and Ge(100), asymmetric dimers being the basic building blocks, and perhaps missing dimer defects being involved. However, we have to remind ourselves that in the experiment² the Sn(100) surface is obtained by molecular-beam epitaxy onto InSb(100), and the role of the

TABLE VI. Optimized atomic positions of the α -Sn(100) $c(4 \times 2)$ -reconstructed surface, and the corresponding bulklike (Ideal) positions. In the oblique supercell (two side lengths of the surface cell are $\sqrt{2} a_0$ and $\sqrt{2.5} a_0$, respectively, and the angle of the two sides is 116.57°), coordinates are given by $\mathbf{r} = c_1 \mathbf{a}_1 + c_2 \mathbf{a}_2 + c_3 \mathbf{a}_3$, where \mathbf{a}_i is defined in the conventional cubic coordinate system as $\mathbf{a}_1 = (a_0/2)(1, 1, 0)$, $\mathbf{a}_2 = (a_0/2)(1, -1, 0)$, and $\mathbf{a}_3 = a_0(0, 0, -1)$ with $a_0 = 12.181$ a.u. = 6.446 \AA the α -Sn lattice parameter. The unit cell has two dimers *A* and *B*.

| | Atom no. | Ideal | | | Optimized | | |
|--------------|----------|-------|-------|-------|-----------|-------|-------|
| | | c_1 | c_2 | c_3 | c_1 | c_2 | c_3 |
| dimer-layer | | | | | | | |
| dimer-A-down | 1 | 0.500 | 0.250 | 1.375 | 0.501 | 0.506 | 1.259 |
| dimer-A-up | 2 | 0.500 | 1.250 | 1.375 | 0.509 | 1.093 | 1.423 |
| dimer-B-up | 3 | 1.500 | 0.250 | 1.375 | 1.500 | 0.421 | 1.424 |
| dimer-B-down | 4 | 1.500 | 1.250 | 1.375 | 1.508 | 1.008 | 1.259 |
| 2nd-layer | | | | | | | |
| | 5 | 0.000 | 0.250 | 1.125 | -0.042 | 0.278 | 1.135 |
| | 6 | 1.000 | 0.250 | 1.125 | 1.042 | 0.278 | 1.134 |
| | 7 | 0.000 | 1.250 | 1.125 | 0.050 | 1.237 | 1.136 |
| | 8 | 1.000 | 1.250 | 1.125 | 0.966 | 1.234 | 1.132 |
| 3rd-layer | | | | | | | |
| | 9 | 0.000 | 0.750 | 0.875 | -0.008 | 0.758 | 0.856 |
| | 10 | 1.000 | 0.750 | 0.875 | 0.993 | 0.756 | 0.854 |
| | 11 | 0.000 | 1.750 | 0.875 | 0.002 | 1.756 | 0.899 |
| | 12 | 1.000 | 1.750 | 0.875 | 0.998 | 1.757 | 0.898 |
| 4th-layer | | | | | | | |
| | 13 | 0.500 | 0.750 | 0.625 | 0.493 | 0.755 | 0.608 |
| | 14 | 1.500 | 0.750 | 0.625 | 1.494 | 0.748 | 0.607 |
| | 15 | 0.500 | 1.750 | 0.625 | 0.500 | 1.754 | 0.639 |
| | 16 | 1.500 | 1.750 | 0.625 | 1.500 | 1.754 | 0.644 |

misfit strain energy could be very important,⁴³ as indicated by successive transformations as a function of epitaxial larger thickness.² It is thus important to understand first the behavior of the substrate-free surfaces.

We therefore carried out a series of surface energy calculations for these possible higher-order reconstruction models, in order to clarify their hierarchy on α -Sn(100). We constructed the atomic configurations starting from the previously calculated symmetric dimer and asymmetric dimer data. We then relaxed the atomic configurations guided by the calculated Hellmann-Feynman forces. Our calculated surface energies for the considered reconstructions are reported in Table II.

A. $c(4 \times 2)$ reconstruction

Ab initio calculations^{27,44} have shown that the $c(4 \times 2)$ reconstruction is the most favorable in Si(100) and Ge(100). The $c(4 \times 2)$ reconstruction is obviously one of the best candidates for the true ground state of α -Sn(100) as well.

We constructed the initial atomic configuration using the asymmetric dimer coordinates (Table IV). At variance with all other cases where the surface unit cell is rectangular, here the surface unit is oblique, and required particular care in the choice of the k -point sampling, as described in Sec. I. The relaxed atomic positions of the top four layers are reported in Table VI. The buckling of the dimer is 1.06 \AA , a little larger than in the 2×1 asymmetric dimer case. The final surface energy is $0.873 \text{ eV}/(1 \times 1 \text{ cell})$, i.e., $39 \text{ meV}/(1 \times 1 \text{ cell})$ lower than that of the 2×1 asymmetric dimer reconstruction.

We mention here that the reflection symmetry through (110) plane in the optimized atomic configuration is slightly broken, as also happened in previous *ab initio* calculations for the $c(4 \times 2)$ reconstruction on Ge(100).⁴⁴ This is attributable to the fact that the k -point integration over the $c(4 \times 2)$ oblique ISBZ cannot be sampled so accurately to preserve this symmetry in an exact manner. However, we do not believe that this slight asymmetry has any consequences, and we shall ignore it.

B. $p(2 \times 2)$ reconstruction

The $p(2 \times 2)$ reconstruction is the other good candidate for the ground state of α -Sn(100). We started our calculation from the atomic configuration constructed through the appropriate arrangement of asymmetric dimers (Table IV), and we relaxed the atoms to the optimal positions. We give the optimized atomic positions of the top four layers in Table VII. The buckling of the dimer is here 1.05 \AA . As expected, the calculated surface energy of $0.872 \text{ eV}/(1 \times 1 \text{ cell})$ is very close (actually, degenerate within our resolution) to that of the $c(4 \times 2)$ reconstruction. These two structures are also calculated to be almost degenerate in Si(100) and Ge(100) surfaces.^{27,28,38,44} Experimental molecular beam epitaxy growth data² show that the $p(2 \times 2)$ structure prevails when the coverage of α -Sn grown on InSb is between 500 and 1000 \AA , while $c(4 \times 2)$ structure is not seen. The reason for this is presently unclear.

In order to provide a comparison with future experiments, we have calculated the electronic band structure and the

TABLE VII. Optimized atomic positions of the α -Sn(100) $p(2 \times 2)$ -reconstructed surface, and the corresponding bulklike (Ideal) positions. In the square supercell, coordinates are given by $\mathbf{r} = c_1 \mathbf{a}_1 + c_2 \mathbf{a}_2 + c_3 \mathbf{a}_3$, where \mathbf{a}_i is defined in the conventional cubic coordinate system as $\mathbf{a}_1 = (a_0/2)(1, 1, 0)$, $\mathbf{a}_2 = (a_0/2)(1, -1, 0)$, and $\mathbf{a}_3 = a_0(0, 0, -1)$, with $a_0 = 12.181$ a.u. = 6.446 Å the α -Sn lattice parameter. The unit cell has two dimers A and B .

| | Atom no. | Ideal | | | Optimized | | |
|--------------|----------|-------|-------|-------|-----------|-------|-------|
| | | c_1 | c_2 | c_3 | c_1 | c_2 | c_3 |
| dimer-layer | | | | | | | |
| dimer-A-down | 1 | 0.500 | 0.250 | 1.375 | 0.500 | 0.505 | 1.267 |
| dimer-A-up | 2 | 0.500 | 1.250 | 1.375 | 0.500 | 1.094 | 1.429 |
| dimer-B-up | 3 | 1.500 | 0.250 | 1.375 | 1.500 | 0.423 | 1.431 |
| dimer-B-down | 4 | 1.500 | 1.250 | 1.375 | 1.500 | 1.009 | 1.266 |
| 2nd-layer | | | | | | | |
| | 5 | 0.000 | 0.250 | 1.125 | -0.044 | 0.279 | 1.140 |
| | 6 | 1.000 | 0.250 | 1.125 | 1.044 | 0.279 | 1.140 |
| | 7 | 0.000 | 1.250 | 1.125 | 0.044 | 1.236 | 1.139 |
| | 8 | 1.000 | 1.250 | 1.125 | 0.956 | 1.236 | 1.139 |
| 3rd-layer | | | | | | | |
| | 9 | 0.000 | 0.750 | 0.875 | -0.001 | 0.757 | 0.859 |
| | 10 | 1.000 | 0.750 | 0.875 | 1.001 | 0.757 | 0.859 |
| | 11 | 0.000 | 1.750 | 0.875 | 0.000 | 1.757 | 0.903 |
| | 12 | 1.000 | 1.750 | 0.875 | 1.000 | 1.757 | 0.903 |
| 4th-layer | | | | | | | |
| | 13 | 0.500 | 0.750 | 0.625 | 0.500 | 0.761 | 0.611 |
| | 14 | 1.500 | 0.750 | 0.625 | 1.500 | 0.743 | 0.609 |
| | 15 | 0.500 | 1.750 | 0.625 | 0.500 | 1.766 | 0.645 |
| | 16 | 1.500 | 1.750 | 0.625 | 1.500 | 1.744 | 0.646 |

core-level shifts of the $p(2 \times 2)$ reconstruction, and reported them in Fig. 10 and Table VIII, respectively. The main features of the band structure are very similar to those observed for the 2×1 asymmetric dimer reconstruction, namely, the filled surface band and empty surface band are separated by a gap of about 1.2 eV, and they both lie in the fundamental gap region of the projected bulk band structure. The surface rocking mode frequency, as well as the surface work function, should be the same, within our accuracy, as those of the 2×1 asymmetric dimer reconstruction.

C. $p(4 \times 1)$ reconstruction

Within the 2×1 family, the $p(4 \times 1)$ reconstruction has, to our knowledge, never been observed in experiments. However, the calculation of the surface energy for this reconstruction, will provide, combined with other 2×1 family reconstructions calculations, relevant information about the

TABLE VIII. Calculated surface core-level shifts on the considered atoms for the $p(2 \times 2)$ reconstruction in the initial- and final-state pictures. The shift is relative to a bulk atom. Units are in eV. Here 2nd-layer atom indicates one of the second layer atoms.

| | Initial state | Final state |
|-----------------|---------------|-------------|
| up-dimer atom | 0.67 | 0.38 |
| down-dimer atom | 0.16 | -0.02 |
| 2nd-layer atom | 0.20 | 0.12 |

interaction structure of dimers on (100) surfaces. This will enable us, in Sec. VII, to predict finite-temperature properties of α -Sn(100) surfaces.

The initial atomic configuration is constructed using the asymmetric dimer coordinates (Table IV), and equilibrium was reached after a short relaxation. The optimized atomic positions of the top six layers are reported in Ref. 23. The buckling of the dimers is 0.964 Å, a little smaller if compared with 2×1 asymmetric dimers. The calculated surface energy is 0.909 eV/(1×1 cell), almost degenerate with the 2×1 asymmetric dimer reconstruction.

We notice that the mirror symmetry about $[1\bar{1}0]$ (the dimer itself is in the $[110]$ direction) between the two dimers, and also that between the atoms in layers below, are slightly lifted (see Ref. 23). This is because the original C_2 symmetry about $[001]$ of a semi-infinite surface is absent in the slab, as in the *ab initio* calculation for Ge(100) in Ref. 44. In Ref. 44, it was confirmed that restoring this symmetry by hand has a negligible effect on the surface energy.

D. $c(2 \times 2)$ reconstruction

Here we consider the $c(2 \times 2)$ family of reconstructions [Fig. 9(b)]. Since it is known that on Si(100) the basic $c(2 \times 2)$ reconstruction has the lowest energy among this family,³⁸ we chose the $c(2 \times 2)$ reconstruction as the representative of the $c(2 \times 2)$ family on α -Sn(100). Since the $c(2 \times 2)$ reconstruction can be made up of symmetric dimers, we first constructed the atomic configuration using the obtained (2×1) symmetric dimer coordinates,²³ then we

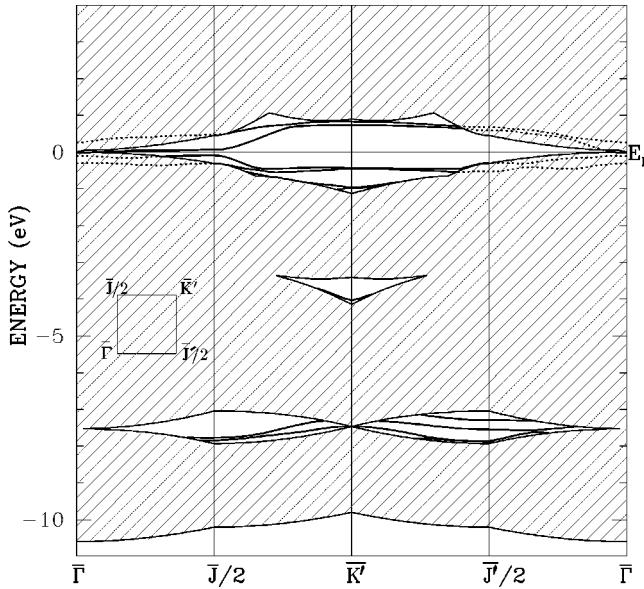


FIG. 10. Surface electronic band structure of the $p(2 \times 2)$ -reconstructed surface reported along high-symmetry lines of the 2×2 square irreducible Brillouin zone. The Fermi level is set to zero. Shaded areas correspond to surface-projected bulk states, while thicker lines correspond to surface states. The irreducible surface Brillouin zone is given in the inset. Note the surface bands in the fundamental gap region, well separated in energy.

relaxed it. The calculated surface energy is $1.008 \text{ eV}/(1 \times 1 \text{ cell})$, slightly lower than that of the 2×1 symmetric dimer reconstruction (Table II), but higher [$0.096 \text{ eV}/(1 \times 1 \text{ cell})$] than that of the 2×1 asymmetric dimer reconstruction (Table II).

Next, we removed the mirror symmetry between the two dimerized atoms, allowed the dimer to become asymmetric, and let the atomic configuration relax to equilibrium. The optimized atomic configuration of the top six layers is reported in Ref. 23. The dimer buckling is 1.03 \AA , almost identical to that of 2×1 asymmetric dimer reconstruction (Table II). The surface energy is $0.907 \text{ eV}/(1 \times 1 \text{ cell})$, which is again almost identical to that of the 2×1 asymmetric dimer reconstruction (Table II). The similarity shown by this calculation between the $c(2 \times 2)$ reconstructions of Sn(100) and Si(100), suggests that other $c(2 \times 2)$ family reconstructions are also not competitive in the search for low-temperature stable phases. We therefore concentrate our attention on the 2×1 family reconstructions.

VII. INTERACTION BETWEEN ASYMMETRIC DIMERS: PHENOMENOLOGICAL

Based on the above results, we can develop a phenomenological model for the interaction among asymmetric dimers which are basic building blocks for the reconstructions on Sn(100). We do this in analogy with the work of Ihm *et al.*³⁸ on Si(100). Two possible orientations can be assigned to the asymmetric dimers. The dimer orientations can therefore be represented by the two possible states of an Ising spin- $\frac{1}{2}$. This is reasonable since the potential barrier for flipping a dimer is as large as 0.12 eV . In this picture, the $c(4 \times 2)$ reconstruction corresponds to the antiferromagnetic phase, the

$p(2 \times 2)$ reconstruction to the layered-antiferromagnetic phase, and so on. Assuming that the energy differences between the possible reconstructions with asymmetric dimers are primarily due to the interaction among the asymmetric dimers, we map these reconstructions onto an effective two-dimensional Ising model, in which the energy differences between different reconstructions are translated into a set of interaction energies of the Ising model. There is a wealth of results available for the two-dimensional Ising model.^{45,46} Using this mapping, it was originally predicted that in Si(100) and Ge(100) surfaces, a second-order phase transition should take place from the ordered reconstruction, $c(4 \times 2)$ or $p(2 \times 2)$, to a disordered 2×1 structure with a transition temperature in the range of $200\text{--}250 \text{ K}$.³⁸ Even if this model is not rich enough to describe in detail the true phase transition [seen experimentally around 170 K on Si(100) and Ge(100) (Refs. 47 and 48)] it does set the right temperature scale. We now investigate that temperature scale for $\alpha\text{-Sn}(100)$.

The following is an effective Ising Hamiltonian corresponding to the 2×1 family reconstructions, which includes all interactions up to twice the surface atom spacing [as illustrated in Fig. 9(a)],³⁸

$$\begin{aligned}
 -\mathcal{H} = & V \sum_{ij} \sigma_{ij} \sigma_{ij+1} + H \sum_{ij} \sigma_{ij} \sigma_{i+1j} \\
 & + D \sum_{ij} \sigma_{ij} \sigma_{i+1j \pm 1} + U \sum_{ij} \sigma_{ij} \sigma_{ij+2} \\
 & + F \sum_{ij} \sigma_{ij} \sigma_{ij+1} \sigma_{i+1j} \sigma_{i+1j+1}, \quad (7)
 \end{aligned}$$

where σ_{ij} is the Ising spin at the lattice site (ij) with two possible values ± 1 . In practice, the couplings U and F can be set to zero since they give the same contribution to the ground-state energy for all considered reconstructions, and also because we lack sufficient information to determine them. The other coupling constants V , H , and D can be extracted from the energy differences among the calculated 2×1 family reconstructions.

Considering the configurations 2×1 , $p(2 \times 2)$, $c(4 \times 2)$, and $p(4 \times 1)$ leads to the following set of equations for the interaction energies per dimer:

$$-\mathcal{H}_{2 \times 1} = V + H + 2D, \quad (8)$$

$$-\mathcal{H}_{p(2 \times 2)} = -V + H - 2D, \quad (9)$$

$$-\mathcal{H}_{c(4 \times 2)} = -V - H + 2D, \quad (10)$$

$$-\mathcal{H}_{p(4 \times 1)} = V - H - 2D. \quad (11)$$

Using the results of Table II, we can extract the coupling constants V , H , and D . One could, at this point, employ renormalization-group or Monte Carlo simulations to calculate and predict the thermodynamic quantities and critical properties. Since we are only interested in the temperature scale that will turn out to be too large, we consider a simpler effective Ising Hamiltonian containing nearest-neighbor interactions only. This is obtained by neglecting D , besides U and F in Hamiltonian (7). In this approximation, the main

contribution to the interaction energies comes from the nearest-neighbor interaction. This simplified Ising Hamiltonian was solved by Onsager. This critical temperature T_c can be obtained⁴⁹ as a solution of the equation

$$|z_1 z_2| + |z_1| + |z_2| = 1, \quad (12)$$

where $z_1 = \tanh(\beta V)$, $z_2 = \tanh(\beta H)$, and $\beta = 1/k_B T$, k_B being the Boltzmann's constant. Now the couplings V and H can be easily derived using the surface energies of the $p(4 \times 1)$, $p(2 \times 2)$, and 2×1 asymmetric dimer reconstructions as

$$V = -40 \text{ meV/dimer}, \quad H = -3 \text{ meV/dimer}. \quad (13)$$

The solution of Eq. (12), obtained using the parameters (13), gives a phase transition temperature, from the ordered, $p(2 \times 2)$ [or $c(4 \times 2)$], reconstruction to a disordered 2×1 phase, roughly of 390 K. This temperature is much higher than the transition temperature of bulk α -Sn into β -Sn (290 K). Even if α -Sn(100) can be clearly stabilized epitaxially on a substrate, as is the case on InSb(100), it seems unlikely that this dimer disordering phase transition might become observable on α -Sn(100).

VIII. WHAT MIGHT THE $c(4 \times 4)$ RECONSTRUCTION BE?

During growth of α -Sn(100) onto InSb(100), a $c(4 \times 4)$ reconstruction was also observed for α -Sn thicknesses between 1000 and 2500 Å.² The nature of this state is presently unknown. A $c(4 \times 4)$ structure was reported on Si(100), but it was shown there to be hydrogen related, without a well-defined structural model.

We first consider the $c(4 \times 4)$ reconstruction without missing dimer defects. It is easy to map the $c(4 \times 4)$ reconstructions onto the effective Ising Hamiltonian (7), and analyze its possibility of competing for the ground state. In Sec. VII we showed that the energy gain of the ordered reconstructed phase mainly arose due to the ‘‘antiferromagnetic-like’’ interaction energy $-V$. Actually, no matter how we arrange the asymmetric dimers in the $c(4 \times 4)$ unit cell, the ‘‘antiferro’’ interaction energies $-V$ are always balanced by the ‘‘ferromagnetic’’ interaction energies V , so that they cancel each other. We can therefore speculate that the surface energy of the $c(4 \times 4)$ reconstructions is close to that of the 2×1 asymmetric dimer reconstruction, and should thus be disfavored for the ground state, as compared with the $p(2 \times 2)$ reconstruction.

In view of the $c(4 \times 4)$ reconstruction reported experimentally, we decided all the same to evaluate microscopically the surface energy for one of these dimer $c(4 \times 4)$ reconstructions. The initial atomic configuration is constructed with the asymmetric buckled dimer coordinates (Table IV). The final relaxed atomic positions of the top six layers are given in Ref. 23. After relaxation, we find that the buckling of dimers is 1.02 Å. The calculated surface energy is 0.903 eV/(1×1 cell), very close to the surface energy of the 2×1 asymmetric dimer reconstruction as expected. We can thus conclude that dimer-based $c(4 \times 4)$ reconstructions are not competitive, at least in unstrained equilibrium.

Next we considered the so-called ‘‘single missing dimer’’

TABLE IX. The magnitude of the buckling, the bond length, and the buckling angle of a dimer in C, Si, Ge, and α -Sn(100) surfaces.

| | Buckling length | Bond length | Buckling angle |
|---------------------------|-----------------|-------------|----------------|
| | (Å) | (Å) | |
| C ^a | 0 | 1.37 | 0° |
| Si ^b | 0.4 | 2.47 | 9° |
| Ge ^c | 0.74 | 2.46 | 17.5° |
| α -Sn ^d | 1.01 | 2.82 | 20.99° |

^aReference 25 (calculated value).

^bReferences 4 and 50 (measured value).

^cReference 51 (measured value).

^dThis work.

$c(4 \times 4)$, where, in the surface $c(4 \times 4)$ cell, one out of four dimers is removed. Several arrangements of a missing dimer defect are possible in a $c(4 \times 4)$ surface cell. However, they are expected to be roughly equivalent in the Ising-spin mapping. For the microscopic calculation, we constructed the initial atomic configuration using the relaxed $c(4 \times 4)$ atomic positions, and removed one dimer. After relaxation, the surface energy of this reconstruction is 0.970 eV/(1×1 cell), which is now substantially *higher* than that of the 2×1 asymmetric dimer reconstruction. In conclusion, none of our attempts provides an explanation for the $c(4 \times 4)$ structure observed on α -Sn(100) grown on InSb(100), which at this stage remains an open problem.

IX. DISCUSSION

We have found that asymmetric dimers are very stable on α -Sn(100), leading to a basic 2×1 unit cell. In higher-order reconstructions, the asymmetric dimers are essentially identical (see Table II), with a similar buckling amplitude (about 1 Å), buckling angles (about 21°), and bond length (about 2.83 Å). Except for the $c(4 \times 2)$ and $p(2 \times 2)$ reconstructions, which are lowest, all surface energies are close within 10 meV/(1×1 cell) with respect to that of the 2×1 asymmetric dimer reconstruction (if we exclude the missing dimer reconstructions which are much higher in energy). Moreover, the electronic band structures of the $p(2 \times 2)$ and 2×1 asymmetric dimer reconstructions are very similar. These all indicate that on α -Sn(100) the asymmetric buckled dimers are rather rigid structures, and the only remaining degree of freedom is in their relative arrangements. Mapping of 2×1 family reconstructions onto an effective Ising model shows that the energy gain of the $c(4 \times 2)$ and $p(2 \times 2)$ reconstructions relative to the 2×1 reconstruction is due to a nearest neighbor ‘‘antiferromagnetic’’ interaction $-V$.

Why do the $c(4 \times 2)$ and $p(2 \times 2)$ reconstructions have the lowest surface energy, at least in the calculations? Physically, it has been shown for Ge(100) surfaces⁴⁴ that the energy gain of the $c(4 \times 2)$ reconstruction with respect to the 2×1 asymmetric dimer one, comes primarily from the relaxations of the atoms in the layer below the dimers. In Ref. 44 two calculations were presented for the $c(4 \times 2)$ reconstruction on Ge(100). In one of them the second-layer atoms were allowed to relax, and in the other one the second-layer atoms were fixed to their corresponding bulk positions. It was

found that the latter was almost degenerate with the 2×1 asymmetric dimer case, but the former brought about an energy gain of 0.05 eV/dimer due to the relaxation of the second-layer atoms. Here we have also done a similar calculation for the α -Sn(100) $p(2 \times 2)$ reconstruction. We fixed the second-layer atoms (of course, including the two innermost layer atoms) in their bulklike positions, and relaxed all other atoms. The surface energy turned out to be 0.07 eV/(1×1 cell) higher than the fully relaxed surface. Checking Tables VI, VII, and IV, we see that for the $c(4 \times 2)$ and $p(2 \times 2)$ reconstructions the atoms in the second layer have free space to move towards the “up” atom of the dimer and away from the “down” atom along the $[1\bar{1}0]$ direction (note that the dimer itself lies in the $[110]$ direction). In $p(2 \times 2)$ or $c(4 \times 2)$ reconstructions they do that in order to keep the bond length close to the bulk value. On the other hand, in the 2×1 asymmetric dimer reconstruction they cannot relax along $[1\bar{1}0]$ due to the constrained geometry. The relaxed positions of the second-layer atoms are, on the other hand, similar for $c(4 \times 2)$ and $p(2 \times 2)$ reconstructions (see Tables VI and VII), which explains why they are energetically so close. The surface energy of the $p(4 \times 1)$ reconstruction is a little lower [3 meV/(1×1 cell)] than that of the 2×1 asymmetric dimer one, which can again be understood by noting that atoms in the second layer have more freedom along the $[110]$ direction in the former.

In conclusion, we have found that a basic 2×1 asymmetric dimer should be responsible for the reconstructions of α -Sn(100). The dimer buckling is predicted to be $\sim 21^\circ$ or $\sim 1 \text{ \AA}$, much larger than the corresponding ones for Si(100)

and Ge(100), which is again in the trend from C to Si, to Ge, and to α -Sn (see Table IX). The associated surface-state gap should be at least 1.2 eV (LDA calculations only provide a lower bound). A surface rocking mode resonance is predicted at 4.8 THz, and should be visible in the surface phonon spectrum at $\vec{k}_{\parallel}=0$. A core-level shift of at least 0.6 eV should also be exhibited by the up-dimer atom. The lowest energy reconstructions are found to be $c(4 \times 2)$ and $p(2 \times 2)$, which are energetically almost degenerate.

Experimental observations on epitaxially grown films of α -Sn(100) on InSb(100) reveal, as a function of increasing thickness, the sequence $2 \times 1 \rightarrow p(2 \times 2) \rightarrow c(4 \times 4)$. We believe we have a good picture for the first two, while we do not understand the $c(4 \times 4)$ structure. The hydrogen-related nature of $c(4 \times 4)$ on Si(100) suggests checking whether impurities might be involved also with their presence in Yuen *et al.*'s growth data.² Another possibility is that the reconstructed α -Sn surface would take on a large surface unit cell to reduce the large strain due to mismatch of growth of α -Sn film on InSb(100) substrate. More work is also needed in order to understand what disfavors the $c(4 \times 2)$ structure relative to the $p(2 \times 2)$ structure, and why the basic 2×1 structure prevails for small thicknesses.

ACKNOWLEDGMENTS

Z.Y.L. thanks Dr. Dario Alfè for useful discussions and his help. This research was partly sponsored by EEC, Contract No. ERBCHRXCT 930342, under Contract No. 95.01056.CT12, and by INFN, through PRA LOTUS.

*Present address: Ames Laboratory—U.S. DOE and Department of Physics and Astronomy, Iowa State University, Ames, Iowa 50011.

¹R. F. C. Farrow, D. S. Robertson, G. M. Williams, A. G. Cullis, G. R. Jones, I. M. Young, and P. N. J. Dennis, *J. Cryst. Growth* **54**, 507 (1981).

²W. T. Yuen, W. K. Liu, B. A. Joyce, and R. A. Stradling, *Semicond. Sci. Technol.* **5**, 373 (1990).

³Winfried Mönch, *Semiconductor Surfaces and Interfaces* (Springer-Verlag, Berlin, 1995).

⁴*Physics of Solid Surfaces*, edited by G. Chiarotti, Landolt-Börnstein, New Series, Group III, Vol. 24, Pt. a (Springer, Berlin, 1993), p. 194.

⁵P. Hohenberg and W. Kohn, *Phys. Rev.* **136**, B864 (1964); W. Kohn and L. J. Sham, *ibid.* **140**, A1135 (1965).

⁶D. M. Ceperley and B. J. Alder, *Phys. Rev. Lett.* **45**, 566 (1980); J. P. Perdew and A. Zunger, *Phys. Rev. B* **23**, 5048 (1981).

⁷R. Stumpf, X. Gonze, and M. Scheffler (unpublished).

⁸L. Kleinman and D. M. Bylander, *Phys. Rev. Lett.* **48**, 1425 (1982).

⁹Zhong-Yi Lu, Guido L. Chiarotti, S. Scandolo, and E. Tosatti, *Phys. Rev. B* **54**, 11 769 (1996).

¹⁰D. L. Rice and J. M. Rowe, *Solid State Commun.* **7**, 1433 (1969).

¹¹S. L. Cunningham, *Phys. Rev. B* **10**, 4988 (1974).

¹²M. Methfessel and A. T. Paxton, *Phys. Rev. B* **40**, 3616 (1989).

¹³V. Fiorentini and M. Methfessel, *J. Phys.: Condens. Matter* **8**, 6525 (1996).

¹⁴O. L. Alerhand and E. J. Mele, *Phys. Rev. B* **35**, 5533 (1987).

¹⁵J. Fritsch and P. Pavone, *Surf. Sci.* **344**, 159 (1995).

¹⁶A. Baldereschi, S. Baroni, and R. Resta, *Phys. Rev. Lett.* **61**, 734 (1988).

¹⁷E. Pehlke and M. Scheffler, *Phys. Rev. Lett.* **71**, 2338 (1993).

¹⁸A. Pasquarello, M. S. Hybertsen, and R. Car, *Phys. Rev. B* **53**, 10 942 (1996).

¹⁹The choice of the radius is somehow artificial. We have tested to adopt radii ranging from 1/3 to 2/3 of the bulk bond length. It turned out that the SCLS values change within 0.06 eV.

²⁰We also used this approach to compute the surface core-level shifts on Si(100), and obtained results similar to those in Ref. 17.

²¹U. Von Barth and R. Car (unpublished).

²²A. Dal Corso, S. Baroni, R. Resta, and S. de Gironcoli, *Phys. Rev. B* **47**, 3588 (1993).

²³Additional details on the calculated reconstructions are given in the Ph.D. thesis by Zhong-Yi Lu, SISSA, Trieste, 1996. This thesis is available via <http://www.sissa.it/cm/CMsector/PHD.html>

²⁴Andrew Zangwill, *Physics at Surfaces* (Cambridge University Press, Cambridge, 1988), p. 94.

²⁵P. Krüger and J. Pollmann, *Phys. Rev. Lett.* **74**, 1155 (1995).

²⁶M. Rohlfling, P. Krüger, and J. Pollmann, *Phys. Rev. B* **52**, 13 753 (1995).

²⁷Z. Zhu, N. Shima, and M. Tsukada, *Phys. Rev. B* **40**, 11 868 (1989).

²⁸N. Roberts and R. J. Needs, *Surf. Sci.* **236**, 112 (1990).

²⁹H. Bilz and W. Kress, *Phonon Dispersion Relations in Insulators*

- (Springer-Verlag, Berlin, 1979).
- ³⁰The adopted sphere radii are somehow arbitrary. We tested the calculations using different radii ranging from half of the bulk bond length to two-thirds of the bulk bond length. The charge transfer in surface states, from the down dimer atom to the up dimer atom, changes correspondingly from $0.3e$ to $0.4e$, while the total charge transfers change from $-0.03e$ to $-0.09e$.
- ³¹R. M. Tromp, R. J. Hamers, and J. E. Demuth, Phys. Rev. Lett. **55**, 1303 (1985), and references therein.
- ³²J. A. Martin, D. E. Savage, W. Moritz, and M. G. Lagally, Phys. Rev. Lett. **56**, 1936 (1986).
- ³³R. J. Hamers, R. M. Tromp, and J. E. Demuth, Phys. Rev. B **34**, 5343 (1986).
- ³⁴J. A. Kubby, J. E. Griffith, R. S. Becker, and J. S. Vickers, Phys. Rev. B **36**, 6079 (1987).
- ³⁵R. S. Becker, B. S. Swartzentruber, and J. S. Visker, J. Vac. Sci. Technol. A **6**, 472 (1988).
- ³⁶H. Wang, R. Lin, and X. Wang, Phys. Rev. B **36**, 7712 (1987).
- ³⁷K. Kato, T. Ide, T. Nishimori, and T. Ichinokawa, Surf. Sci. **207**, 177 (1988).
- ³⁸J. Ihm, D. H. Lee, J. D. Joannopoulos, and J. J. Xiong, Phys. Rev. Lett. **51**, 1872 (1983).
- ³⁹K. C. Pandey, in *Proceedings of the International Conference on the Physics of Semiconductors*, edited by D. J. Chadi and W. A. Harrison (Springer, New York, 1985), p. 55.
- ⁴⁰I. P. Ipatova, Yu. E. Kitaev, and A. V. Subashiev, Surf. Sci. **110**, 543 (1981).
- ⁴¹V. E. Zubkus, P. J. Kundrotas, S. N. Molotkov, V. V. Zatarsi, and E. E. Tornau, Surf. Sci. **243**, 295 (1991).
- ⁴²G. J. R. Jones and B. W. Holland, Solid State Commun. **46**, 651 (1983).
- ⁴³J. C. Phillips, Phys. Rev. Lett. **45**, 905 (1980).
- ⁴⁴M. Needels, M. C. Payne, and J. D. Joannopoulos, Phys. Rev. Lett. **58**, 1765 (1987).
- ⁴⁵J. M. van Leeuwen, Phys. Rev. Lett. **34**, 1056 (1975).
- ⁴⁶*Phase Transition and Critical Phenomena*, edited by C. Domb and M. S. Green (Academic, New York, 1976), Vol. 6.
- ⁴⁷S. D. Kevan and N. G. Stoffel, Phys. Rev. Lett. **53**, 702 (1984).
- ⁴⁸T. Tabata, T. Aruga, and Y. Murata, Surf. Sci. **179**, L63 (1987).
- ⁴⁹Barry M. McCoy and Tai-Tsun Wu, *The Two-Dimensional Ising Model* (Harvard University Press, Cambridge, MA, 1973), pp. 89 and 90.
- ⁵⁰B. W. Holland, Surf. Sci. **140**, L269 (1984).
- ⁵¹R. Rossmann, H. L. Meyerheim, V. Jahns, J. Wever, W. Moritz, D. Wolf, D. Dornisch, and H. Schulz, Surf. Sci. **279**, 199 (1992).